Molecular Therapy
Original Article

RTN4 Knockdown Dysregulates the AKT Pathway, Destabilizes the Cytoskeleton, and Enhances Paclitaxel-Induced Cytotoxicity in Cancers

Gopal P. Pathak,[1] Rashmi Shah,[1] Barry E. Kennedy,[1] J. Patrick Murphy,[1] Derek Clements,[1] Prathyusha Konda,[1] Michael Giacomantonio,[1] Zhaolin Xu,[1] Isabel R. Schlaepfer,[3] and Shashi Gujar[1,2,4,5]

[1]Department of Pathology, Dalhousie University, Halifax, NS B3H 1X5, Canada; [2]Department of Microbiology and Immunology, Dalhousie University, Halifax, NS B3H 1X5, Canada; [3]Division of Medical Oncology, Genitourinary Cancer Program, University of Colorado School of Medicine, Aurora, CO 80045, USA; [4]Department of Biology, Dalhousie University, Halifax, NS B3H 1X5, Canada; [5]Centre for Innovative and Collaborative Health Systems Research, IWK Health Centre, Halifax, NS B3K 6R8, Canada

Reticulon-4 (RTN4), commonly known as a neurite outgrowth inhibitor (Nogo), is emerging as an important player in human cancers. Clinically, we found lower RTN4 expression in patient-derived tumors was associated with significantly better survival in lung, breast, cervical, and renal cancer patients. To identify the role of RTN4 in cancer biology, we performed mass spectrometry-based quantitative proteomic analysis on cancer cells following RTN4 knockdown and found its link with pro-survival as well as cytoskeleton-related processes. Subsequent mechanistic investigations revealed that RTN4 regulates lipid homeostasis, AKT signaling, and cytoskeleton modulation. In particular, downregulation of RTN4 reduced sphingomyelin synthesis and impaired plasma membrane localization of AKT, wherein AKT phosphorylation, involved in many cancers, was significantly reduced without any comparable effect on AKT-related upstream kinases, in a sphingolipid-dependent manner. Furthermore, knockdown of RTN4 retarded proliferation of cancer cells *in vitro* as well as tumor xenografts in mice. Finally, RTN4 knockdown affected tubulin stability and promoted higher cytotoxic effects with chemotherapeutic paclitaxel in cancer cells both *in vitro* and *in vivo*. In summary, RTN4 is involved in carcinogenesis and represents a molecular candidate that may be targeted to achieve desired antitumor effects in clinics.

INTRODUCTION

Chemotherapy is still by far the most frequently practiced first line of cancer treatment in clinics; however, several cancers develop resistance to chemotherapies over time through various mechanisms.[1] For effective cancer treatment, continuous development of new therapeutic targets through deeper mechanistic insights on the process of carcinogenesis to enhance the sensitivity of cancer cells to chemotherapeutics is imperative. Fortunately, targeted therapies and application of combinatorial therapeutic approaches, in conjunction with the discovery of new molecular targets, have shown promising outcomes.[2–4] Furthermore, recent technological advances in proteomics approaches have streamlined the identification of molecular targets that play a critical role in oncogenic pathways and thus are amenable to therapeutic modulations. Previously, using mass spectrometry-based cell surface protein analysis, we identified a relationship between Reticulon-4 (RTN4) and immune suppression in Ras oncogene-based cell transformations pointing toward a possible role for RTN4 in cancers.[5] However, the precise role for RTN4 in cancer biology or its therapeutic implications for cancer therapy have remained poorly understood.

The RTN4 or neurite outgrowth inhibitor (Nogo) protein family contains three major isoforms: RTN4A (Nogo A), RTN4B (Nogo B), and RTN4C (Nogo C).[6,7] The three isoforms of Nogo share a common 188-aa C-terminal membrane-spanning domain, known as a reticulon homology domain. RTN4A is the largest of the Nogo isoforms, which has been studied extensively in the context of the CNS. It functions as a myelin-associated inhibitor of axon regeneration and is responsible for the inhibition of neurite outgrowth and neuronal plasticity.[7] In terms of tissue-specific expression of isoforms, RTN4A is mostly expressed in the CNS, whereas RTN4C is found in the CNS and in skeletal muscles. Alternatively, RTN4B expression is found in several tissues, where it regulates important cellular events including angiogenesis, macrophage movement, vascular modeling, sphingolipid homeostasis, inflammation, and immune responses.[8–14] In endothelial cells, RTN4B regulates *de novo* synthesis of sphingosine-1-phosphate (S1P) by inhibiting serine palmitoyl transferase.[10,15] RTN4B is also associated with pathological conditions including pulmonary arterial hypertension (PAH)[8] and hepatic fibrosis,[16] in which it is reported to promote cell proliferation. In vascular endothelial cells[17] and human monocyte-derived macrophage cells,[18] RTN4B modulates cytoskeleton and is a key player in their motility.[13,19]

Received 7 January 2018; accepted 31 May 2018;
https://doi.org/10.1016/j.ymthe.2018.05.026.

Correspondence: Shashi Gujar, DVM, PhD, MHA, Departments of Pathology, Microbiology and Immunology, and Biology, Dalhousie University, Rm. 11J Sir Charles Tupper Medical Building, 5850 College Street, Halifax, NS B3H 1X5, Canada.
E-mail: shashi.gujar@dal.ca

We recently showed that RTN4B negatively affects the interferon response in oncogene-transformed cells and thus contributes to cancer-associated immune suppression.[5]. This hypothesized role for RTN4 in carcinogenesis was further supported by recent reports that documented aberrant expression of RTN4B in hepatocellular carcinoma (HCC)[20] and identified it, through a chemoproteomics approach, as a druggable target in colorectal cancer.[21] Interestingly, RTN4B has been found in caveolae and lipid rafts[9] and shown to be functionally associated with phospholipids.[8,10,15] Since the activation of AKT, a major signaling molecule with pro-oncogenic activities, is affected in response to the perturbations within lipid homeostasis, there exists a possibility that RTN4 regulates the AKT pathway. However, the role for RTN4 in the regulation of AKT remains unknown. Of note, membrane raft nanodomains formed by cholesterol and sphingolipids play a crucial role in the activation of phosphatidylinositol 3-kinase (PI3K)/AKT pathway by facilitating AKT recruitment and phosphatidylinositol (3,4,5)-trisphosphate (PIP3) accumulation in the plasma membrane, where AKT phosphorylation takes place.[22] Such subcellular localization of RTN4 can be of a special significance in terms of AKT activation, as PI3K/AKT is a well-characterized growth factor response pathway associated with important cellular and pathophysiological features required for carcinogenesis.[23–26] However, the mechanistic details connecting RTN4 to AKT-related signaling in oncogenesis and its therapeutic relevance are unclear.

In the current study, using quantitative proteomics coupled with molecular validations, we find that RTN4 regulates phospholipid homeostasis, AKT signaling, and cytoskeleton stability. Our data show that RTN4 knockdown (KD) significantly hampers the capacity of cancer cells to proliferate and form tumors when xenografted in mice. Importantly, clinical relevance for RTN4 is recapitulated in the patient-derived tumors, wherein lower expression of RTN4 is associated with better survival from lung, breast, cervical, and renal cancers. Finally, we show that downregulation of RTN4 results in alteration of microtubule dynamics, consequently promoting higher cytotoxicity in cancer cells when combined with cytoskeleton-targeting chemotherapy agent paclitaxel. Taken together, these findings suggest a novel role for RTN4 in cancer and identify RTN4 as a potential target with translational implications.

RESULTS

Expression of RTN4 Inversely Correlates with Survival from a Variety of Cancers

First, to understand the clinical relevance of RTN4 in human cancers, we evaluated the mRNA profiles of various patient-derived tumor samples that are publicly available in The Cancer Genome Atlas (TCGA) domain.[27,28] Kaplan-Meier survival analysis with the datasets from lung, breast, cervical, kidney, and ovarian patients revealed an inverse relationship between RTN4 expression and overall survival (Figure 1). In all these five cancer datasets, Cox proportional-hazard analysis revealed a hazard ratio of higher than 5, indicating that groups with higher RTN4 expression are 5 times more at risk compared to groups with lower RTN4 expression. These findings strongly suggest a relationship between RTN4 expression and patient survival in different cancers. Taken together, our analysis of patient-derived tumors identified the therapeutic potential for RTN4 inhibition in cancer.

Quantitative Multiplexed Proteomics Reveals a Role for RTN4 in Cell Division, Cytoskeleton Dynamics, and Lipid Biosynthetic Pathways

Since we observed that low RTN4 expression correlates with better patient outcomes, we next investigated the effect of RTN4 inhibition on the cancer cell proteome. To unbiasedly understand these effects, we first performed a quantitative proteome analysis of MCF7 breast cancer cells following RTN4 KD compared to wild-type control. RTN4 KD was achieved by lentiviral-based small hairpin RNA (shRNA) targeting the 3′ specific to RTN4 (C terminus of reticulon homology domain). We used tandem mass tag (TMT)-based, quantitative mass spectrometry[29,30] (Figure 2A) and focused on understanding whether cancer cells express any specific isoform of RTN4. We were able to quantify three peptides specific to RTN4, one of which exclusively belonged to RTN4 isoform B (in the splicing site specific to RTN4B), whereas two other peptides were from the reticulon homology domain commonly shared by RTN4A, RTN4B, and RTN4C isoforms (Figure 2B). This peptide quantification showed the presence of RTN4B isoform in MCF7 cells, without ruling out the possibility for RTN4A and RTN4C expression. To dissect the RTN4 isoform expression patterns, we performed immunoblot analysis, using an antibody that identifies both RTN4A and RTNB isoforms, on MCF7, along with other breast (MDA-MB-468 and MDA-MB-231) and lung (H1299 and A549) cancer cell lines and found that the tested cell lines mostly expressed RTN4B, whereas we did not detect RTN4A (Figure S1). In addition, immunoblot analysis of H1299 and MDA-MB-231 cells, using an antibody targeting the C-terminal reticulon homology domain, also validated the presence of only RTN4B in these cell lines (Figure S1). Together, in agreement with the previous reports outlining RTN4B as the major RTN4 isoform in various non-neuronal cells, our proteomics and immunoblot analysis data suggest that the epithelial cancer cells predominantly express RTN4B.

Overall, our proteomic analysis quantified 2,768 proteins from MCF7 cells. By correlating the reduced RTN4 protein expression with all other proteins identified in these cells, we found that numerous proteins have a positive or negative correlation with RTN4 (Figure 2C), indicating that RTN4 KD globally affects many cellular pathways. We performed gene ontology (GO) term analysis on the strong positively ($R > 0.7$) as well as negatively correlated protein ($R < -0.7$) groups. Next, Panther statistical overrepresentation analysis for GO terms was performed to infer particular categories of proteins, belonging to specific biological processes enriched in these groups. With a false discovery rate (FDR) threshold of <0.05, we observed that various GO biological process terms were significantly enriched in each group. To summarize, the significantly enriched GO terms of the biological process ontology were

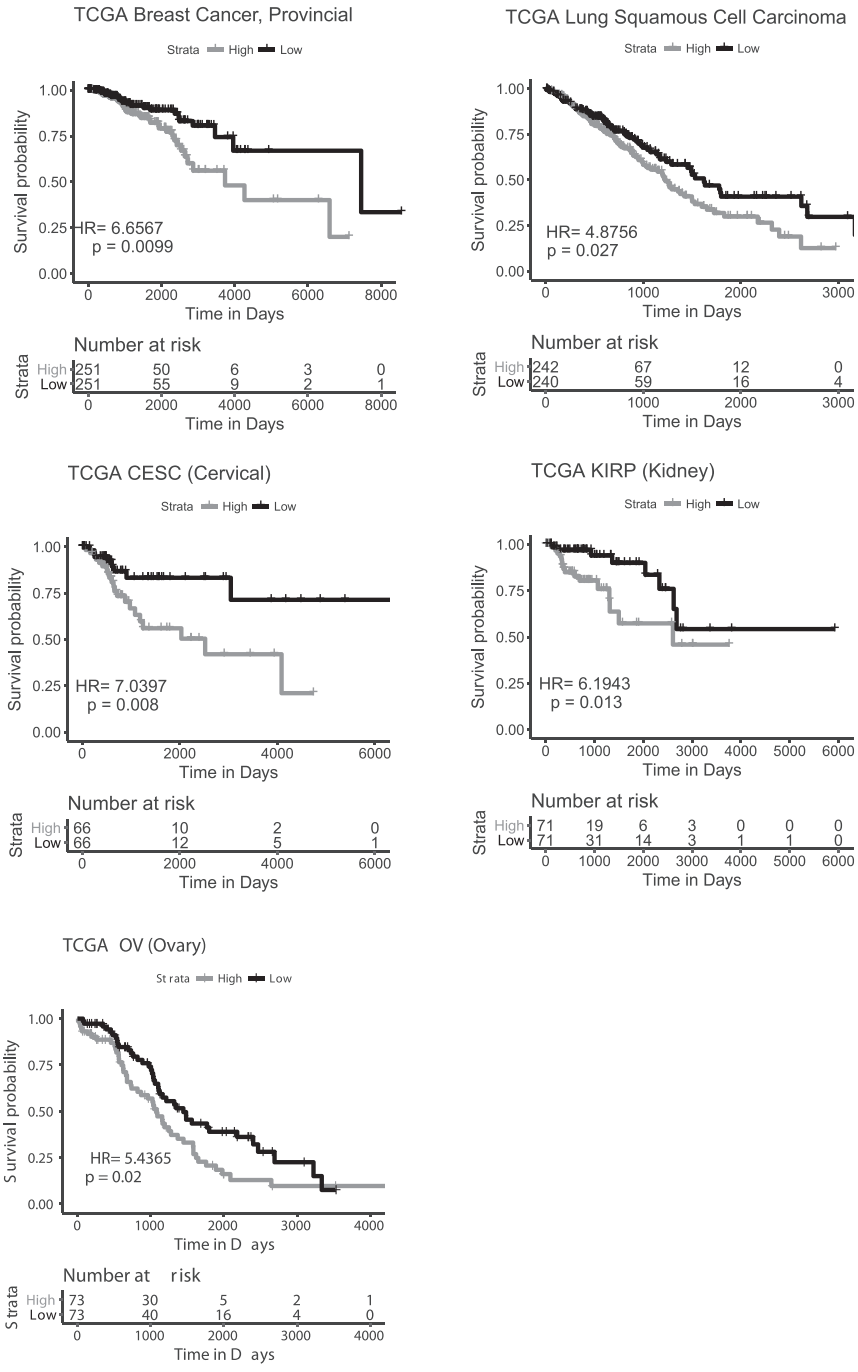

Figure 1. RTN4 Expression Correlates to Poor Prognosis

Kaplan-Meier survival curves for RTN4 in different TCGA datasets. Survival probability is plotted against time (in days) with respect to the high (red) or low (blue) expression of RTN4. Strata showing the number at risk at every time point. KIRP, kidney renal papillary cell carcinoma; CESC, cervical squamous cell carcinoma and endocervical adenocarcinoma; OV, ovarian serous cystadenocarcinoma; HR, hazard ratio. p = log rank t test p value.

represented on 2D semantic space (Figures 2D and 2E). The graphs show FDR values on the x axis and semantic space Y or plot Y values generated using REVIGO,[31] on the y axis. This analysis showed that the positively correlated groups included pathways associated with cell death/apoptosis, cell division, cytoskeleton-based processes, and fatty acid beta oxidation (Figure 2D). Among the negatively correlated proteins, we observed enriched expression of proteins belonging to cell homeostasis, cholesterol biosynthesis, lipid biosynthesis pathways, cytoskeleton, as well as negative regulation of apoptotic and mitotic processes (Figure 2E). We then compared the log fold changes of the proteins belonging to certain pathways of interest, to understand the rate at which they are being modified upon RTN4 KD (Figures 2F and 2G). We also found a significant decrease in the components of the Arp2 and 3 complex in RTN4 KD cells (Figure S2). In summary, our proteomic analysis revealed a connection between RTN4 and cytoskeleton, cell division, and lipid-metabolism processes.

Dysregulated AKT Pathway Accompanies RTN4 KD-Induced Inhibition of Cell Proliferation

Reports suggest that RTN4B is associated with diverse pathological conditions and that the upregulation of the protein suppresses apoptosis and promotes hyper-proliferation of cells in PAH[8] and hepatic fibrosis.[16] To investigate such implications in cancer cell proliferation, we performed RTN4 KD in a panel of lung and breast cancer cell lines (Figure S3A) and then analyzed these cells with a carboxyfluorescein succinimidyl ester (CFSE)-based proliferation assay by fluorescence-activated cell sorting (FACS). We found that RTN4 KD significantly reduced cell proliferation in all cancer cell lines studied (Figures 3A and S3B), as was evident with higher residual CFSE fluorescence in RTN4 KD cells compared to their respective controls. In line with the recent report,[20] these results demonstrated the antiproliferative effects of RTN4 KD.

Next, we investigated mechanisms by which RTN4 might affect cancer cell proliferation. First, we focused on understanding the link between RTN4 and the AKT pathway, as (1) the AKT pathway

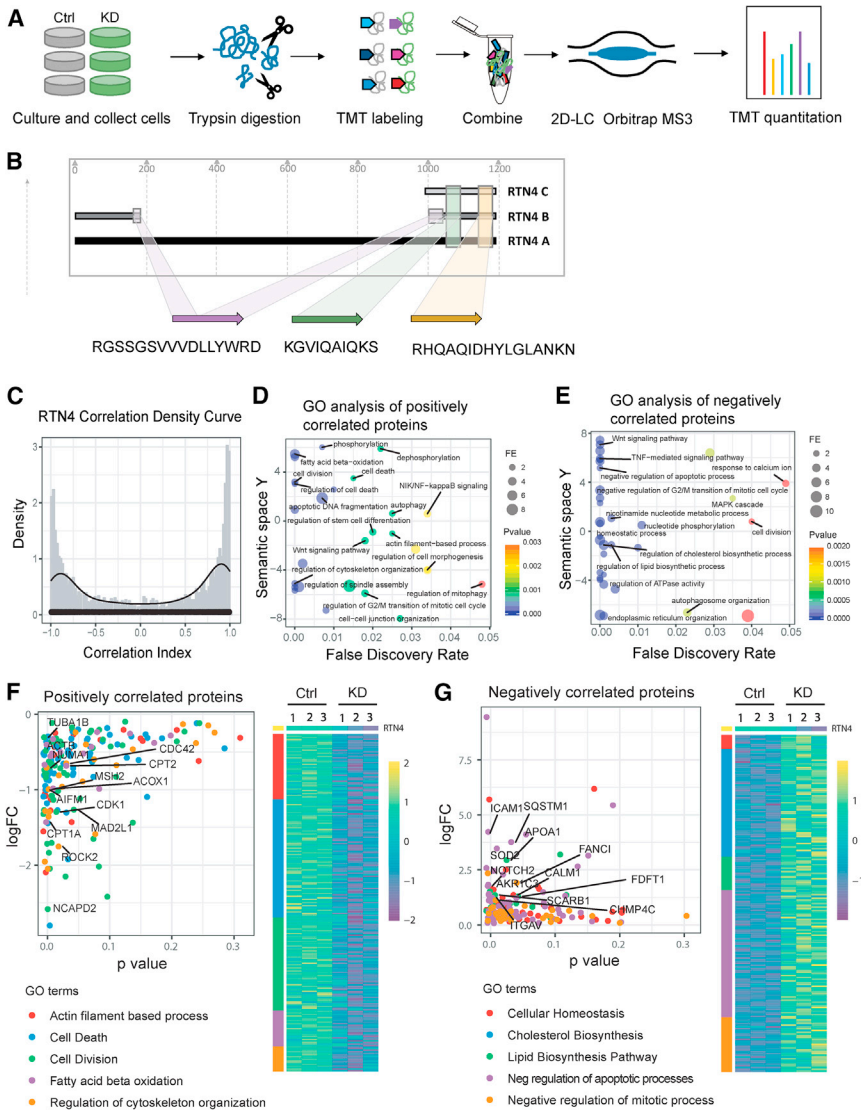

Figure 2. Proteomic Analysis of MCF Cells with Reference to RTN4

(A) Schematic diagram representing 6-plex TMT proteomics workflow. (B) Graphical representation of the RTN4-specific peptides quantified by liquid chromatography-tandem mass spectrometry (LC-MS/MS) and their alignment with isoforms of RTN4. (C) Correlation density plot of RTN4 expression with expression of all other proteins identified in the dataset. (D and E) GO term analysis of positively (D) and negatively (E) correlated proteins with respect to RTN4. (F and G) Comparative GO term analysis of positively (F) and negatively (G) correlated proteins playing a role in various cellular processes of interest. Graphs show logFC (KD or control) on y axis and p value on x axis for proteins belonging to different GO terms, all color coded based on the group. The heatmaps show the expression profiles (*Z* scores) of all the proteins in associated GO categories. Ctrl, control; KD, RTN4 KD; FE, fold enrichment.

is an important regulator of cell growth, proliferation, motility, and survival, and (2) RTN4 localizes in caveolae and lipid rafts (CEM/LR),[9,22] which are known to be important in AKT pathway regulation. For this, we knocked down RTN4 in H1299 (lung) and MDA-MB-231 (breast) cancer cell lines. As shown in Figures 3B and 3C, both H1299 and MDA-MB-231 cells with RTN4 KD contained significantly lower levels of phosphorylated AKT, without effecting total AKT levels, as compared to the respective controls. These results confirm that RTN4 KD impairs phosphorylation of AKT, and suggest a role for RTN4 in AKT activation. In line with this hypothesis, analysis of the downstream protein p21, which is negatively regulated by the AKT pathway,[32] demonstrated higher levels of p21 in RTN4 KD cells as compared to the controls (Figures 3D and 3E). However, phospho-p21, which is positively regulated by activated AKT, was significantly reduced in RTN4 KD cells, further supporting the RTN4 KD-mediated impairment of AKT activation (Figures 3D–3G).

Next, to elucidate the mechanistic link between RTN4 and the AKT pathway, we analyzed the level of upstream activators of the AKT pathway by immunoblotting. As shown in Figures S4A and S4B, we were unable to find any significant change in the levels of phospho-PI3K and phospho-pyruvate dehydrogenase kinase 1 (PDK1) between cells with and without RTN4 KD. Similar results were also observed for PI3K/AKT pathway inhibitor phospho-phosphatase and tensin homolog (PTEN) (Figure S4C). These results suggested the possible involvement of non-canonical molecular pathways of AKT regulation following RTN4 KD. AKT is phosphorylated in the PIP3-rich plasma membrane, and for this event to take place, membrane localization of AKT is necessary.[33] Therefore, we next investigated the localization of AKT in the context of RTN4 KD. Since membrane localization of AKT is facilitated by pleckstrin homology (PH) domain of AKT, which binds to the PIP3-rich region of plasma membrane,[33] we tested whether RTN4 KD affected membrane localization of AKT. For this purpose, we constructed a GFP-fused AKT1PH (PH domain of AKT1) protein (AKT1PH-GFP) that localizes to the membrane upon activation of PI3K/AKT pathway. As shown in Figures 3H and 3I, AKT1PH-GFP localized to membrane in control, but not in RTN4 KD H1299 and MDA-MB-231 cells after serum starvation and subsequent stimulation with growth media supplemented with insulin, demonstrating that RTN4 KD impairs the ability of AKT1PH to localize to membrane. Similarly, phosphorylation of endogenous AKT was also impaired in RTN4 KD H1299 cells (Figures 3J and 3K) even when the cells were cultured in the similar stimulatory conditions as used in Figure 3H. These observations demonstrated that loss of RTN4 impairs the membrane localization of AKT and

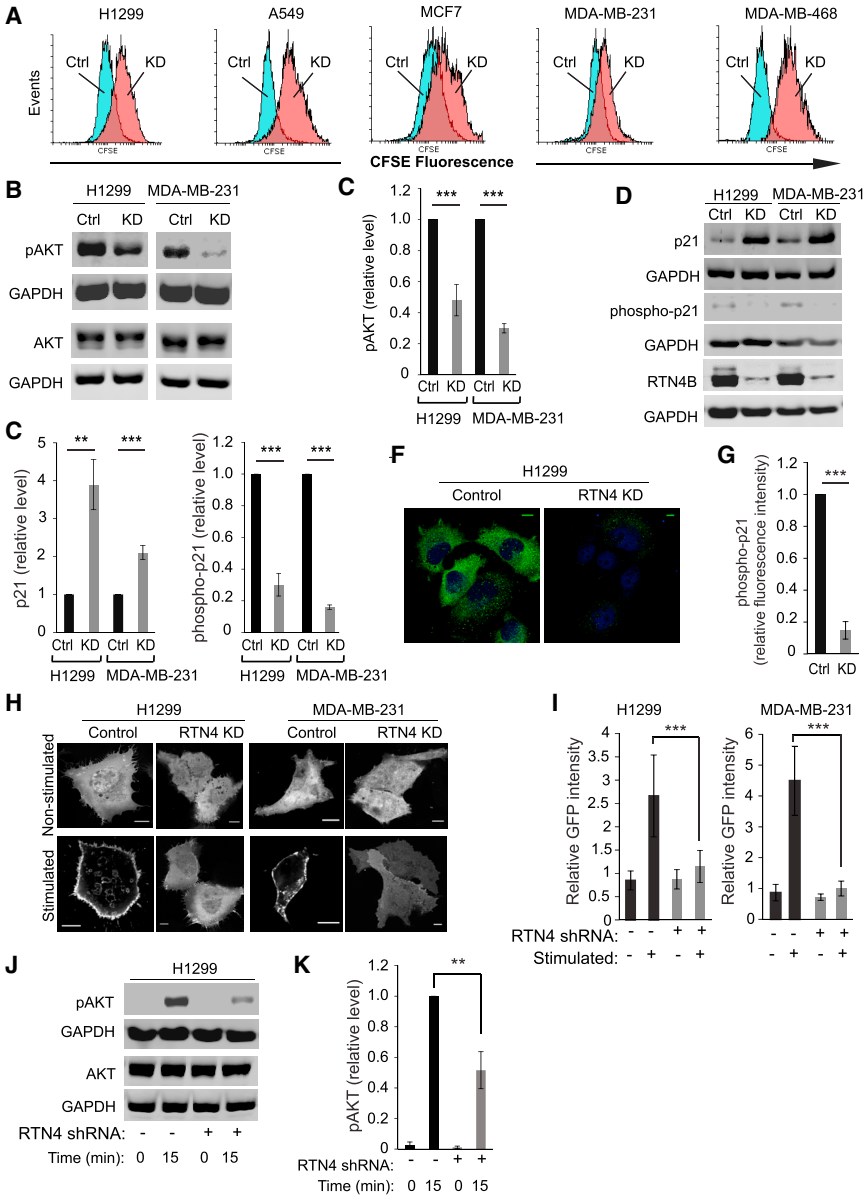

Figure 3. RTN4 KD Retards Cancer Cell Proliferation and Dysregulates the AKT Pathway

(A) CFSE-based proliferation assay of selected human lung and breast cancer cell lines (H1299, A549, MCF7, MDA-MB-231, and MDA-MB-468) with stably expressing RTN4-shRNA (KD) or control (Ctrl). Cells, stained with CFSE, were grown for 4 days and analyzed by flow cytometry to determine cell proliferation. In this assay, CFSE fluorescence gets halved in proliferating daughter cells, and thus fast-growing cells bear less fluorescence than the slow-growing cells. CFSE fluorescence histogram plot of control (blue histogram) and RTN4 KD (pink histogram) after 4 days of culture are shown as overlay histograms. (B) Immunoblots showing the effect of RTN4 downregulation on phospho-AKT (Ser 473) in H1299 and MDA-MB-231. (C) Quantification of change in the level of phospho-AKT (Ser 473) in RTN4 KD cells compared to control (from immunoblot analysis, normalized with AKT). Data presented as mean ± SD (n = 3). (D) Immunoblot image showing total and phospho-p21 protein level in control and RTN4 KD cells. (E) Quantification of change in the level of p21 and phospho-p21 in RTN4 KD cells compared to control (from immunoblot analysis). Data presented as mean ± SD (n = 3). (F) Immunofluorescence image of control and RTN4 KD H1299 cells showing the effect of RTN4 downregulation in the level of phospho-p21. Green, phospho-p21; blue, TOPRO3 nuclear stain (scale bar, 10 μm). (G) Quantification of fluorescence intensity of phospho-p21 (green) in control and RTN4 KD H1299 cells (normalized to the nuclear staining). Data presented as mean ± SD (n = 10). (H) Images showing the effect of RTN4 KD in translocation of AKT1PH-GFP in plasma membrane in H1299 and MDA-MB-231 cells. Cells were transiently transfected with AKT1PH-GFP, serum starved for 8 hr, and stimulated with 25 μg/mL of insulin in growth media for 15 min and fixed. Scale bars, 10 μm. (I) Ratio of localization of AKT1PH-GFP in membrane to cytosol per cell in control and RTN4KD cells as illustrated in (H) (n = 10). (J) Endogenous phospho-AKT (Ser 473) in serum-starved and stimulated control and RTN4 KD H1299 cells. Cells were serum starved for 8 hr and harvested (0 min) or stimulated with 25 μg/mL of insulin in growth media for 15 min and harvested for immunoblot analysis. (K) Quantification of level of pAKT (normalized with AKT) from immunoblot analysis as in (J). Data presented as mean ± SD (n = 3). **0.001 < p ≤ 0.01; ***p ≤ 0.001.

ultimately its phosphorylation. Together with previous data, these results show that inhibition of RTN4 promotes reduced cell proliferation at least partially through the AKT pathway.

RTN4 KD Disrupts AKT Membrane Localization through Impaired Sphingomyelin Homeostasis

Our data thus far pointed out that RTN4 modulates AKT trafficking to the cell membrane. Furthermore, our proteomic analysis also showed that RTN4 is associated with cholesterol and lipid biosynthetic pathways. It should be noted that, in neurons, RTN4 is associated with the formation of myelin,[34] which is composed of cholesterol and lipids, including sphingomyelins.[35] Interestingly, sphingomyelin is a major sphingolipid that plays a crucial role in AKT membrane recruitment and phosphorylation.[22] In this context, we reasoned that RTN4 could regulate phospholipids, including sphingomyelins, which may explain the defective localization and subsequent decrease in phosphorylation of AKT in cancer cells following RTN4 KD. To assess this hypothesis, we carried out mass spectrometry (MS)-based lipidomics analysis in H1299 cells following RTN4 KD. First, the comparative MS analysis of lipid content between control and RTN4 KD H1299 cells showed that the triacylglycerol (TAG) levels within RTN4 KD cells were lower than that of control H1299 cells (Figure 4A). Strikingly, in phospholipid analysis, we observed a significant decrease in sphingomyelin levels in cells with RTN4 KD

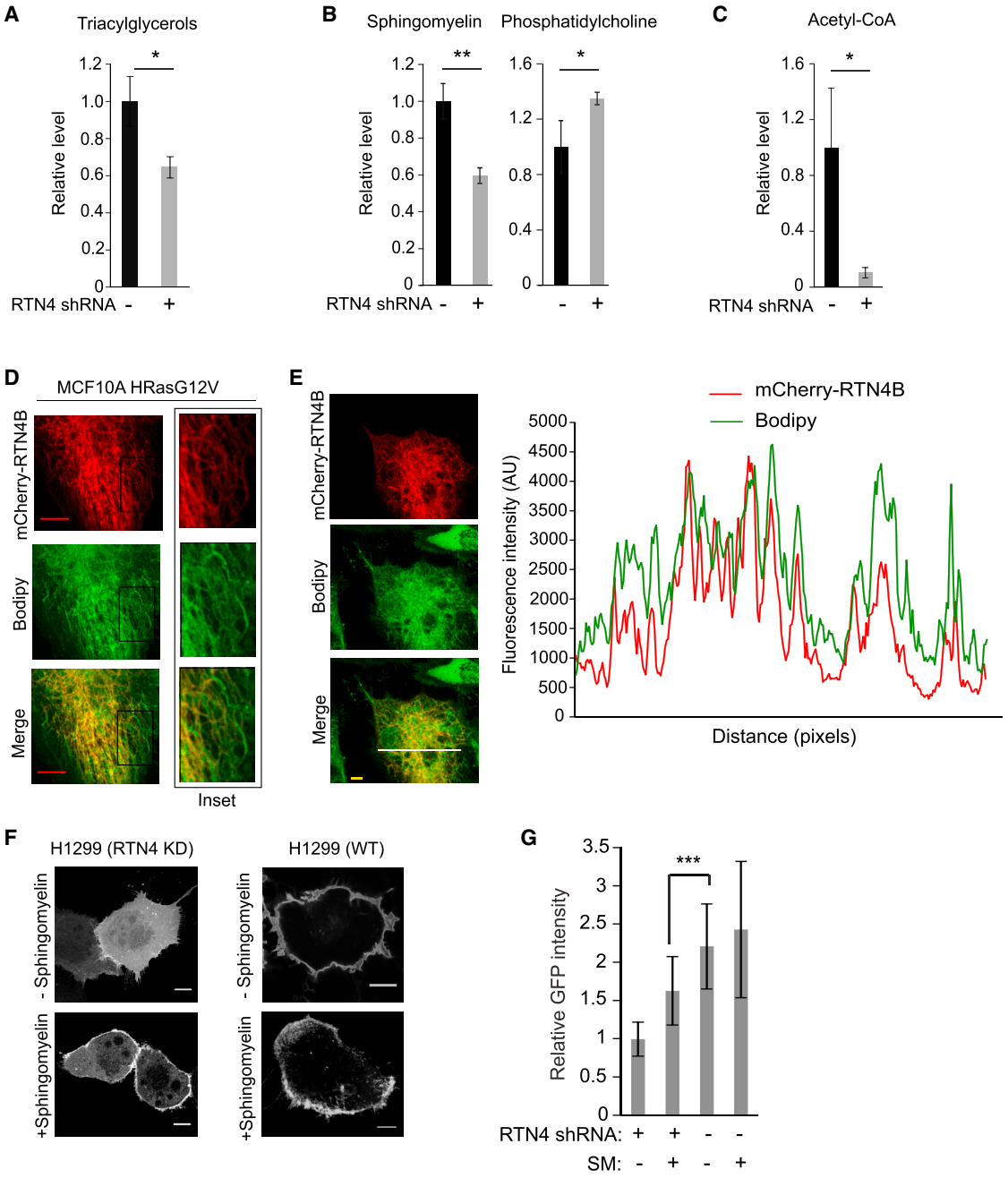

Figure 4. RTN4 Regulates Lipid Homeostasis

(A) Total triacylglyceride level in control and RTN4 KD H1299 cells. Data presented as mean ± SD (n = 3). (B) Total sphingomyelin and phospatidylcholine in control and RTN4 KD H1299 cells. Data presented as mean ± SD (n = 3). (C) Relative level of acetyl-CoA in control and RTN4 KD H1299 cells shown as peak height determined by quantitative metabolomic analysis. Individual data plotted in graph (n = 2, from each control and RTN4 KD). (D) Live cell images showing the association of mCherry-RTN4B with lipids (green). MCF10A-HRasG12V cells were transiently transfected with mCherry-RTN4B and labeled with Bodipy FL C12 for 4 hr, and live confocal images were taken. Degree of co-localization in the selected region (rectangular box as shown in the inset) calculated by Pearson's correlation coefficient (R) = 0.80. Scale bars, 10 μm. (E) Fluorescence intensity profile plotted from the image containing fluorophores mCherry-RTN4B and Bodipy FL C12 as shown (along the white line) to show their co-occurrence. The fluorescence peak of mCherry-RTN4B appears closer to Bodipy (green). Degree of co-localization calculated by Pearson's correlation coefficient (R) = 0.84. Scale bars, 5 μm.

(legend continued on next page)

compared to the controls (Figure 4B). In agreement with these data, we also observed higher levels of phosphatidylcholine (a precursor of sphingomyelin) in RTN4 KD cells compared to the control cells (Figure 4B). Next, to understand the effect of RTN4 KD on the cellular global metabolome, we performed targeted metabolomics with hydrophilic interaction liquid chromatography MS (HILIC-MS) on H1299 cells with or without RTN4 KD.[36] Supporting our data thus far, our metabolomics analysis captured a decrease in acetyl-coenzyme A (CoA), which is an important factor in lipid synthesis, following RTN4 KD in cancer cells (Figure 4C). Together, these data demonstrated that the inhibition of RTN4 results in altered sphingolipid homeostasis.

To gain insight into the relationship between RTN4 and lipid transport, which might influence sphingomyelin homeostasis, we tested the interaction of RTN4B with lipids. Previous reports have indicated a role for RTN4B in the transfer of phospholipids to the mitochondria from endoplasmic reticulum.[8] Sphingomyelin synthesis occurs by the transfer of phosphocholine group from phosphatidylcholine to ceramide, and at least two members of sphingomyelin synthases (SMS1 and SMS2) are involved in this process.[37] To assess the possible role of RTN4 in phospholipid transfer, we engineered mCherry-tagged RTN4B (mCherry-RTN4B) and transiently expressed it in MCF10A cells. We performed confocal analysis of cells expressing mCherry-RTN4B after treatment with fluorescent phospholipid precursor dye Bodipy FL C_{12}. As shown in Figures 4D and 4E, mCherry-RTN4B co-occurs with fluorescently labeled lipids. Together, and in line with previous reports,[8] our live cell imaging shows that RTN4B co-occurs with lipids and possibly is involved in lipid transfer.

Finally, to conclusively demonstrate the role of RTN4 KD-mediated reduced sphingomyelin levels on AKT membrane localization, we exogenously supplied the sphingomyelin to wild-type and RTN4 KD H1299 cells that were transiently transfected with AKT1PH-GFP. Strikingly, cells with RTN4 KD partially restored the membrane recruitment of AKT1PH-GFP after supplemented with exogenous sphingomyelin (Figures 4F and 4G). These data conclusively show that RTN4 KD-mediated decreased sphingomyelin impedes AKT localization, which could be rescued through the supplementation of exogenous sphingomyelins. Together, these results demonstrate that RTN4 regulates AKT membrane recruitment through the modulation of sphingomyelin homeostasis through a yet unknown mechanism.

RTN4 Inhibition Destabilizes Microtubules and Cytoskeleton Dynamics

Since our proteomic analysis revealed a link between RTN4B and cytoskeleton and considering the importance of cytoskeleton dynamics in cell division, we next evaluated the effect of RTN4 KD on microtubules. Dynamic localization of RTN4B and its interaction with tubulin play a role in movement of migratory cells,[17,18] where RTN4 is found to localize into cell protrusions.[18] To gain further insight about the role of RTN4 in regulating cytoskeleton dynamics, we carried out immunofluorescence analysis focusing on RTN4 and α-tubulin. We found that RTN4 is distributed near tubulin (Figures 5A and S5A) as reported earlier.[18] Interestingly, as compared to control cells, the cells with RTN4 KD displayed change in cell morphology that was further highlighted by tubulin cytoskeleton rearrangement (Figure 5A). In addition, the pattern of tubulin localization was changed in cells with RTN4 KD (Figures 5A, 5B, and S5B). This implication of RTN4 on tubulin led us to study its effect on tubulin acetylation in cancer cells. As shown in Figures 5C and 5D, RTN4 KD in lung (H1299, A549) as well as breast (MCF7, MDA-MB-468) cancer cell lines resulted in the decreased levels of acetylated tubulin, with no effect on total tubulin. Interestingly, compared to normal MCF10A, oncogenic *ras*-transformed MCF10A contained higher levels of acetylated tubulin, which was decreased following RTN4 KD, supporting the role of RTN4 in regulating tubulin acetylation in cancer cells (Figures 5E and 5F). In line with the established correlation between tubulin acetylation and microtubule stability,[38] these data strongly suggested that RTN4 KD destabilizes tubulins.

Recently, membrane protrusions, known as microtentacles, have been shown to be associated with aggressiveness and metastatic behavior of cancer cells.[39] As our study showed impact of RTN4 KD on AKT pathway and tubulin cytoskeleton, we wanted to know the effect of RTN4 KD on microtentacles. For this purpose, wild-type or RTN4 KD H1299 cells were transiently transfected with GFP, and microtentacles were visualized in suspended cells by live cell confocal imaging. We found that H1299 with RTN4 KD displayed drastic reduction in number and size of the microtentacles as compared to the control (Figures S6A and S6B, shown by arrowheads). These results suggest that RTN4 is involved in the regulation of microtentacle formation. Our data (Figures S6C and S6D) showed that H1299 cells with RTN4 KD migrated slower than that of wild-type cells and suggested that decreased RTN4 expression can reduce migratory properties, known to be necessary for invasion and metastatic potential, of cancer cells. Together, these data suggested a role for RTN4 in regulating microtentacles involved in cancer aggressiveness.

RTN4 Inhibition Enhances the Susceptibility of Cancer Cells to Chemotherapeutic Paclitaxel

We next wanted to investigate whether the change in microtubule stability induced by RTN4 inhibition can be used to improve the outcome of the cytoskeleton-targeting anticancer drugs. For this purpose, we chose a commonly used chemotherapeutic paclitaxel, a drug that causes mitotic arrest and cell death by impeding microtubule

(F) RTN4 KD H1299 cells transfected with AKT1PH-GFP were grown with or without 25 μM sphingomyelin for 16 hr and serum starved for 8 hr. Cells incubated with sphingomyelin were supplemented with sphingomyelin during serum starvation. After serum starvation cells were stimulated with 25 μg/mL of insulin in growth medium for 15 min and fixed. Scale bars, 10 μm; Ctrl, control (wild type with empty vector); KD, RTN4 KD. (G) Ratio of localization of AKT1PH-GFP in membrane to cytosol per cell in control and RTN4KD cells as illustrated in (F) (n = 10). *$0.01 < p \leq 0.05$; **$0.001 < p \leq 0.01$; ***$p \leq 0.001$.

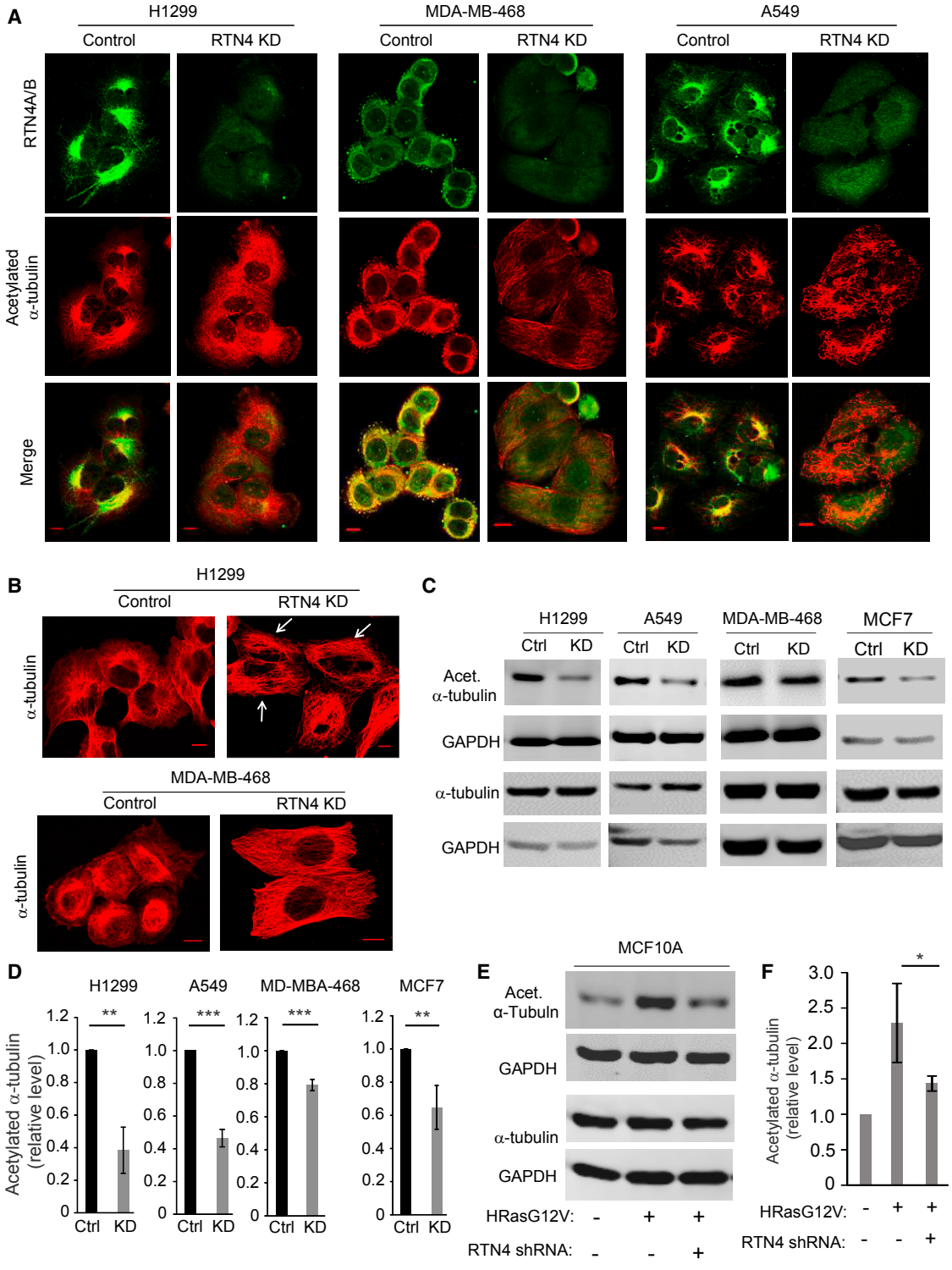

Figure 5. RTN4 KD Impacts Tubulin Cytoskeleton

(A) Immunofluorescence images showing effect of RTN4 downregulation on acetylated α-tubulin organization. In control cells, acetylated α-tubulin co-occurs with RTN4 predominantly in perinuclear region, which after RTN4 KD changes the pattern of organization. (B) Effect of RTN4 KD on α-tubulin. The tubulin filaments lose their perinuclear pattern of localization in RTN4 KD cells. (Scale bars, 10 μm). Antibody targeting RTN4 in immunofluorescence analysis detects RTN4A and B isoforms only. (C) Immunoblots

(legend continued on next page)

dynamics.[40] Previous reports have shown that AKT activation is associated with taxol resistance in cancer cells in clinical settings.[41–43] As our data demonstrated that RTN4 KD reduced AKT activation and destabilized tubulin, we hypothesized that RTN4 KD would enhance the cytotoxic effect of paclitaxel in cancer cells and thus allow for the development of a novel combinatorial anticancer therapeutic approach. To investigate this, we treated five different cell lines with or without RTN4 KD. As shown in Figure 6A, the susceptibility of cancer cells to paclitaxel increased after RTN4 KD. All the tested cell lines showed the highest reduction in cell survival with a RTN4 KD + paclitaxel combination, compared to any of the other mono- or combination strategies tested. Surprisingly, MCF7 cells, which are less susceptible to paclitaxel compared to other cell lines, became readily susceptible to the drug after RTN4 ablation (Figure 6A). These results demonstrated that RTN4 KD in combination with paclitaxel decreases cancer cell survival more efficiently than RTN4 KD or paclitaxel alone.

Finally, and in line with our observations with RTN4 KD-enhanced paclitaxel-based cytotoxicity (Figure 6A), we asked whether RTN4 KD in combination with paclitaxel could be used to improve the outcomes from cancers *in vivo* in a preclinical setting. To investigate this, we tested the efficacy of paclitaxel in targeting human tumors, with or without RTN4 KD, xenografted in NOD-SCID mice. For this purpose, H1299 cancer cells were injected subcutaneously in NOD-SCID as per schematic shown in Figure 6B and then additionally treated with paclitaxel (7.5 mg/kg of body weight; intraperitoneal) on 4 consecutive days, starting from day 27 post-tumor xenograft. As shown in Figure 6C, animals grafted with RTN4 KD cells and injected with paclitaxel (RTN4 KD + paclitaxel) showed the highest, and statistically significant, survival advantage on day 49 post-tumor xenograft compared to any other experimental condition tested (wild-type [WT], RTN4 KD alone or WT + paclitaxel combination). These data conclusively demonstrate the antitumorigenic effects of RTN4 inhibition in cancers in a preclinical, *in vivo* setting. Further, it also suggests that microtubule-destabilizing effects of RTN4 KD can be combined with microtubule-targeting chemotherapeutics to enhance the chemotherapeutic effects of taxols. Collectively, these data clearly demonstrate that RTN4 KD impairs the proliferation of cancer cells and most importantly, combined with the antimicrotubule agent paclitaxel, offers a novel approach to achieve better antitumor outcomes *in vitro* and *in vivo*.

DISCUSSION

In this study, we report a novel role for RTN4 in tumorigenesis and describe a previously uncharacterized relationship between RTN4 and chemotherapy. The clinically relevant aspect of RTN4 is readily evident in patient-derived tumors, as a lower expression of RTN4 mRNA in multiple types of cancers predicts better overall survival for patients. Mechanistically, our data demonstrate that RTN4 regulates cancer cell proliferation through dysregulations within AKT pathway activation that are accompanied by aberrant phospholipid homeostasis and cytoskeleton destabilization. Most importantly, and in line with the growing appreciation of combinatorial therapeutic strategies for cancer therapy,[2] we show that RTN4 downregulation in combination with paclitaxel promotes greater antitumor effects *in vitro* and *in vivo*. These findings put forward clinically relevant anticancer implications for RTN4.

Involvement of RTN4 in cancer growth and survival remains poorly understood. Our data from CFSE-based proliferation as well as cell-counting assays support the notion that RTN4 is essential for the proliferation and survival of breast and lung cancer cells. Similar implications for RTN4 are evident in several pathophysiological conditions such as PAH,[8] liver fibrosis,[16] and hepatocellular carcinoma cells.[20] In line with these pro-survival activities in cancer cells, we discovered that the genetic downregulation of RTN4 expression results in reduced AKT activation that is an important signaling event associated with tumorigenesis and metastatis.[23] Furthermore, increased phosphorylation of AKT (Ser 473) has been shown to correlate with the cancer aggression and poor clinical outcome.[44] It can be further surmised that RTN4 KD impairs phosphorylation of AKT, which further supports the pro-survival role of RTN4 in cancer cells.

Of note, RTN4 KD-mediated AKT modulation existed without any significant variation in the levels of upstream activators PI3K and PDK or negative regulator PTEN. These observations prompted us to investigate non-canonical regulators of the AKT pathway, such as molecules involved in its trafficking. Our comprehensive lipidomic analysis identified reduced sphingomyelin levels in RTN4 KD cells, which also showed impaired membrane recruitment of AKT1PH-GFP. Our data suggest that RTN4 modulates AKT pathway by regulating sphingomyelin homeostasis and facilitating AKT membrane recruitment. This phenomenon can have broad implications in cell fate and survival as various signaling molecules regulating cellular activities are generated from sphingomyelin in plasma membrane by sphingomyelinases in response to the wide array of signaling cues. Sphingomyelin is an important constituent of lipid raft nanodomains that facilitates AKT recruitment and accumulation of PIP3 in the plasma membrane.[22] Its role in AKT phosphorylation has been demonstrated, wherein the chemical inhibition of sphingomyelin abrogates the localization of AKT to the plasma membrane and impairs its phosphorylation.[22] Similarly, genetic silencing of SMS1 gene has been shown to impair AKT phosphorylation and proliferation in neuronal[45] as well as HeLa cervical cancer cells.[46] Thus, it is highly likely that RTN4 modulates membrane rafts[9] via sphingomyelin.

showing the effect of RTN4 KD in tubulin acetylation in lung and breast cancer cell lines. Control (Ctrl) cells, RTN4 downregulated (KD) cells were probed for total and acetylated α-tubulin. (D) Quantification of acetylated α-tubulin in RTN4 KD cells compared to the controls (normalized with α-tubulin). Data presented as mean ± SD (n = 3). (E) Change in level of acetylated α-tubulin in wild-type, *ras*-transformed, and *ras*-transformed + RTN4 KD MCF10A normal breast cells. (F) Quantification of acetylated α-tubulin (normalized with α-tubulin) in cells as illustrated in (E). Data presented as mean ± SD (n = 3). *$0.01 < p \leq 0.05$; **$0.001 < p \leq 0.01$; ***$p \leq 0.001$.

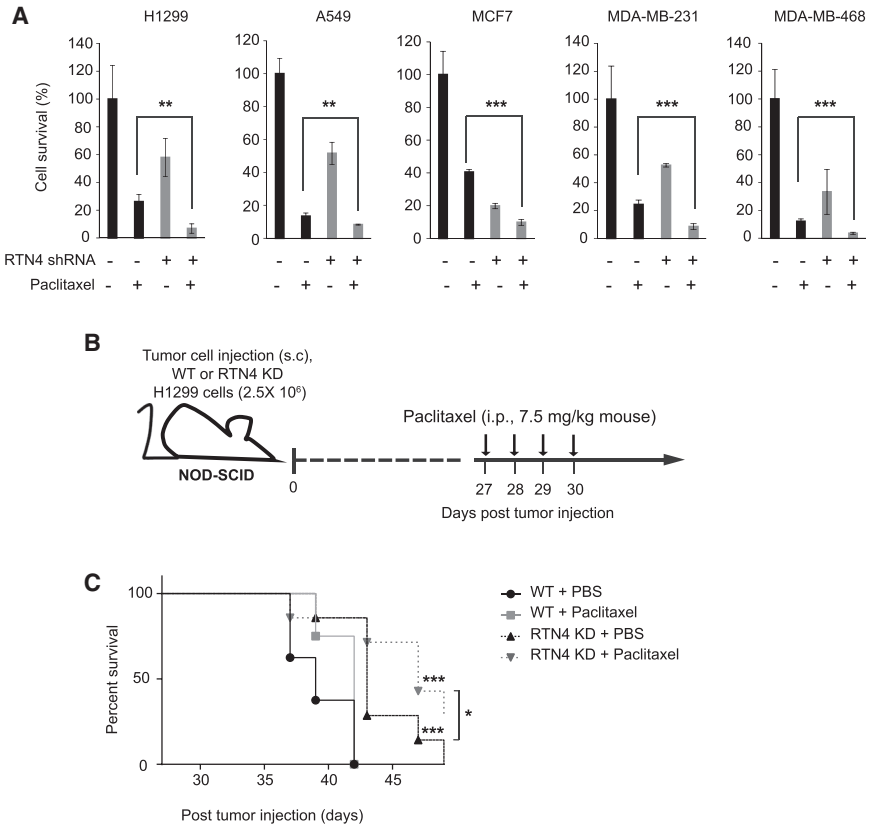

Figure 6. RTN4 KD Impairs Tumorigenesis and Promotes Higher Cytotoxic Effects with Paclitaxel

(A) 100,000 cells, either control or RTN4 KD, each from H1299, A549, MDA-MB-231, MDA-MB-468, and MCF7 were seeded to each well of 12-well dishes. Cells were supplemented with 500 nM of paclitaxel after 16 hr, grown for an additional 48 hr and then counted. Data shown as % change compared to the untreated control cells. Data presented as mean ± SD (n = 3). (B) Schematic showing the *in vivo* tumor development assay. NOD-SCID mice were injected with wild-type or RTN4 KD H1299 cells subcutaneously. Starting from day 27 paclitaxel or placebo was administered for 4 consecutive days and survival was monitored. (C) Graph showing number of mice xenografted with WT or RTN4 KD H1299 cells alive at different time points post-paclitaxel injection. (n = 8 for wild-type xenografts; n = 7 for RTN4 KD xenografts). NOD-SCID mice were injected with WT or RTN4 KD H1299 cells subcutaneously. Once tumor formed (day 27), paclitaxel was injected intraperitoneally (i.p.) for 4 consecutive days. p values between WT (PBS) and RTN4 KD (PBS), and WT (paclitaxel) and RTN4 KD (paclitaxel) is shown on top of each RTN4 KD line. *0.01 < p ≤ 0.05; **0.001 < p ≤ 0.01; ***p ≤ 0.001.

SMS1 and SMS2 synthesize sphingomyelin from ceramide, a membrane-bound molecule generated in endoplasmic reticulum, which needs to be transported between the membranes because of its very low solubility in aqueous environment.[37] Ceramide trafficking is carried out by either vesicular transport or through ceramide transfer protein. Our imaging results provide evidence of association and a likely interaction of RTN4 with lipids. Moreover, an increased level of phosphatidylcholine, a precursor of sphingomyelin in RTN4 KD cells (Figure 4B), also suggests the role of RTN4 in sphingomyelin synthesis. It is plausible that impairment of trafficking of the precursor to the site of synthesis can contribute to the reduced level of sphingomyelin synthesis in the absence of RTN4. In agreement with this function, previous reports have also indicated its role in phospholipid transfer from endoplasmic reticulum.[8] RTN4B inhibits conversion of 3-keto-sphinganine to ceramide, and the depletion of RTN4 leads to an increase in ceramide in endothelial cells.[10] Interestingly, accumulation of ceramide or ceramide analogs has been shown to negatively regulate the AKT pathway and affect mitochondrial functions,[47,48] further supporting the antiproliferating effect of RTN4 KD. In our experiments, although exogenously supplied sphingomyelin could partially rescue the membrane recruitment of AKT1PH-GFP in RTN4 KD cells, a rescue of the phosphorylation of endogenous AKT was not observed in such cells (Figures S7A and S7B), indicating a role of phospholipid homeostasis in AKT activation through a yet-unknown mechanism. As RTN4 contributes to the formation of lipid-rich nanodomains[9] and co-occurs with lipids as shown in our study, future studies are needed to investigate the relation of RTN4 and its interaction with phospholipids in detail. As RTN4 KD causes significant antiproliferative effects in cancer cells, a combination of drugs targeting mitochondrial dynamics with RTN4 KD may be used to inhibit pro-survival mechanism and potentiate mitochondrial signaling in some pathological conditions. Specifically, as RTN4 affects mitochondrial polarization and apoptotic signaling in conditions such as PAH,[8] it would be of interest to study the agents that target mitochondrial homeostasis in combination with RTN4.[48,49]

In the present study, we show that the KD of RTN4 results in destabilization of tubulin cytoskeleton and loss of microtentacles and membrane projections. Cancer cells are characterized by altered tubulin posttranslational modifications.[39] Microtentacles and tubulin projections develop due to cytoskeletal imbalances as a result of the force of outwardly expanding microtubules overcoming the contractile force exerted by actin.[50] Such cytoskeletal aberrations are common in cancers and have been shown to contribute in their invasiveness and dissemination.[50] Interestingly, downregulation of RTN4 resulted in reduced tubulin acetylation in lung cancer and oncogene-transformed MCF10A cells. Further, in addition to the strong co-occurrence of RTN4 with acetylated tubulin, we also observed that downregulation of RTN4 caused the decrease in the level of acetyl-CoA, the metabolite needed for tubulin acetylation.[38,51] This decrease in acetyl-CoA is likely due to reduced fat oxidation since CPT1A, the rate-limiting step in beta-oxidation, is significantly decreased in RTN4 KD cells (Figure 2F). Moreover,

AKT has been shown to regulate microtubule stability,[52] thus suggesting a possible impact of RTN4 KD on tubulin via the dysregulated AKT pathway. Of note, RTN4's association with the cytoskeleton has been demonstrated in macrophages and vascular endothelial cells,[17,18] wherein its localization in filopodia and cell protrusions are crucial in macrophage migration and infiltration.[18] Interestingly, the involvement of RTN4 in cancer cytoskeleton dynamics was further strengthened by our proteomic analysis, which revealed a significant impact of RTN4 KD in the Arp2 and 3 protein complexes, a known modulator of actin cytoskeleton, cell polarity, cell migration, and protrusion.[53–55] Besides the impact of acetyl-CoA on the cytoskeleton, its role as an energy source from lipids to promote RTN4-mediated cell filopodia, protrusions, and migration warrants further investigation.

Finally, our results demonstrate RTN4 has clear translational implications, which was further supported by RTN4 expression and patient survival outcome. Next, we defined that the effects of RTN4 ablation in cancer cells could be used to increase the susceptibility of cancer cells to paclitaxel. Many cytoskeleton-targeting chemotherapeutics are extensively used in cancer treatment. Paclitaxel, one such a commonly used drug, augments microtubule stability and inhibits tubulin dynamics and causes cancer cell death. This drug has been proven effective against various cancer types; however, many cancers, especially advance-staged, show limited susceptibility to paclitaxel. A multitude of mechanisms, including AKT pathway activation, have been described for the resistance of cancer to paclitaxel.[41–43,56] More importantly, administration of paclitaxel itself has been shown to cause an increase in AKT pathway in tumors, conferring drug resistance in clinical settings.[41–43] Since RTN4 modulates tubulin stability (Figures 5 and S5), our data supports a model where blockade of RTN4 in combination with paclitaxel would be a more effective therapeutic treatment. Additionally, we observed that RTN4 KD showed enhanced cytotoxic effects of paclitaxel in various types of cancers *in vitro*, which could be further recapitulated in a xenografted human lung cancer model *in vivo*. Together, our analysis of a patient-derived tumor sample database, combined with *in vitro* and *in vivo* experiments, supported that RTN4 favors oncogenic progression and thus is of clinical relevance.[48,49]

In summary, we report that RTN4 expression inversely predicts survival from lung, breast, cervical, kidney, and ovarian cancers and that its inhibition negatively affects cell proliferation through dysregulation of cytoskeleton and AKT pathways. These RTN4 KD-mediated effects can be combined with paclitaxel to promote even greater antitumor effects *in vivo*. These data identify both prognostic and therapeutic potential of RTN4 in the management of cancers in clinics.

MATERIALS AND METHODS

Plasmids and Constructs

mCherry-RTN4B was constructed by inserting RTN4B in *Bsrg*I and *Not*I sites of mCherry-N1 (Clontech). Sequence coding RTN4B was amplified from RTN4A-GFP in two steps, one from the N-terminal common region and the other from the C-terminal homology region. Both fragments were assembled by overlapping PCR with *Bsrg*I and *Not*I restriction sites in each end. AKT1-PH domain (1–164 aa) was amplified from human cDNA and cloned into enhanced green fluorescent protein in N1 vector (pEGFPN1) (Clontech) linearized by *Nhe*I and *Bam*HI digestion to construct AKT1PH-GFP. RTN4A-GFP was a gift from Gia Voeltz (Addgene plasmid #61807). pBabe-HRasG12V was a gift from Dr. Bob Weinberg (Addgene plasmid #1768). pLKO.1 empty vector (backbone vector used for RTN4 shRNA) control (used as wild-type control) and pLKO-RTN4-shRNA (TRCN0000071688) were purchased from GE Dharmacon. A list of gene-specific primers used in this study is presented in Table S1.

Cell Culture and Virus Preparation

HEK293T, MCF7, MDA-MB-231, and MDA-MB-468 cell lines were maintained in DMEM supplemented with 10% FBS and 1% Antibiotic-Antimycotic (Gibco). H1299 cells were maintained in Roswell Park Memorial Institute (RPMI) 1640 medium supplemented with 10% fetal bovine serum (FBS) and 1% Antibiotic-Antimycotic (Gibco); A549 cell lines were maintained in minimum essential medium (MEM) supplemented with 10% FBS and 1% Antibiotic-Antimycotic (Gibco). MCF10A cell lines were maintained at DMEM F12 medium supplemented with 5% horse serum, 20 ng/mL of epidermal growth factor (EGF), 0.5 μg/mL hydrocortizone, 100 ng/mL of cholera toxin, 10 μg/mL of insulin, and 1% Antibiotic-Antimycotic (Gibco). All cell lines were maintained at 37°C with 5% CO_2. HEK293T cells were transfected using calcium phosphate or Lipofectamine 2000 (Invitrogen). Transient transfection of other cells was performed using Lipofectamine 2000 (Invitrogen), according to the manufacturer's protocol. For lentivirus or retrovirus preparation, lenti- or retroviral plasmids were co-transfected with packaging and envelop plasmids into HEK293T cells. Supernatant containing viruses was harvested after 36 hr of transfection, then filtered with 0.45 μM filter, and stored at −80°C. Stable cell lines prepared from lentiviral or retroviral transfection were selected using puromycin (2 μg/mL).

Analysis of Phospholipids by Mass Spectrometry

Lipidomic analysis was performed at the Mass Spectrometry Lipidomics Core Facility, University of Colorado, Anschutz Medical Campus (Aurora, CO). After extracting lipids using the Bligh and Dyer method, phospholipids were analyzed by liquid chromatography-tandem mass spectrometry as described.[57,58] Data were analyzed using MultiQuant software from AB Sciex (Framingham, MA) and are presented as the ratios between the integrated area of the peak intensity of each analyte and the peak intensity of the corresponding internal standard.

Metabolomic and Quantitative Proteomic Analysis with Mass Spectrometry

For metabolomics, metabolites were extracted from cells by scraping in ice-cold (−20°C) 80% methanol. Samples were centrifuged at 13,000 × *g* for 5 min, and a 25-μL aliquot of supernatant was added

to 225 μL of HILIC loading solvent containing 95% acetonitrile, 2 mM ammonium hydroxide, and 2 mM ammonium acetate then centrifuged again at 13,000 × *g* for 5 min. Triplicate 50-μL injections of the supernatant were loaded on an Acquity UPLC BEH Amide, 1.7 μm particle size, 2.1 × 100-mm column. Multiple reaction monitoring (MRM) was performed using a Sciex 5500 QTRAP using a previously described acquisition method.[36] Peak heights for individual metabolites were extracted using Multiquant Software. Proteomic analysis was performed using 10-plex TMTs with an MS/MS/MS (MS3) method.[59,60] In brief, pelleted cells were lysed in 2% SDS, 150 mM NaCl, 50 mM Tris (pH 8.5) containing protease inhibitor cocktail. Lysis was performed using a probe sonicator for 12 s on ice. Lysates were cleared by centrifugation at 13,000 × *g* for 5 min, and protein concentrations were determined using a bicinchoninic acid (BCA) assay (Thermo-Fisher Scientific, Rochford, IL). Cysteine residues were reduced using 5 mM dithiothreitol for 40 min at room temperature, then alkylated using 14 mM iodoacetamide for 40 min in the dark followed by methanol chloroform precipitation. The protein was resuspended in 8 M urea and 50 mM Tris, and protein concentration was assessed using a BCA assay. Aliquots containing 100 μg of protein were diluted to 1 M urea, 50 mM HEPES (pH 8.5) and digested overnight with trypsin (Promega, Madison, WI) at a ratio of 1:100 trypsin/protein, then again at a ratio of 1:100 trypsin/protein for 4 hr. Digested peptides were desalted using 60 mg solid-phase C18 extraction cartridges (Waters, Milford, MA) and lyophilized. Dried peptides were labeled using six-plex TMT reagents (Thermo-Fisher Scientific, Rochford IL), mixed equally, desalted using solid-phase C18 extraction cartridges (Waters, Milford, MA), and lyophilized. TMT6-labeled samples were fractionated using high-pH reversed phase chromatography performed with an Onyx monolithic 100 × 4.6 mm C18 column (Phenomenex, Torrance, CA). The flow rate was 800 μL/min and a gradient of 5% to 40% acetonitrile (10 mM ammonium formate [pH 8]) was applied over 60 min using an Agilent 1100 pump (Agilent), from which 12 fractions were collected. Fractions were desalted using homemade stage tips and lyophilized. Each fraction was analyzed using an Orbitrap Velos Pro mass spectrometer (Thermo-Fisher Scientific, Rochford IL) using an MS3 method as previously described.[59,60] Protein identification was performed using a database search against a human proteome database concatenated to a database of common proteomic contaminants. All FDR filtering and protein quantitation was performed as previously described.[59,60]

For computational analysis, the proteomics database was divided into two groups based on their correlation value with RTN4, positively (>0.7) and negatively (<−0.7) correlated proteins. GO analysis was performed on these groups using the Panther database. GO biological processes analysis was performed under statistical enrichment, with default parameters. GO terms with FDR <0.05 and fold enrichment ≥2 were then analyzed using Revigo, to create a semantic 2D space to project these GO terms. Selective GO terms and proteins belonging were then analyzed for logFC versus p value changes. Heatmaps were generated using *Z* scores. All graphs were plotted using R.

Chemical and Drug Treatments

For the AKT membrane localization study, cells were serum starved for 8 hr and stimulated with 25 μg/mL of insulin in the regular growth medium. For sphingomyelin supplementation, cells were grown for 24 hr in the presence of 25 μM sphingomyelin C-12SM (Sigma) in the growth medium. For cellular treatment, paclitaxel was prepared in DMSO (10 mg/mL). Clinical grade injectable paclitaxel (Biolyse Pharma) was diluted in 1× PBS for *in vivo* use.

CFSE-Based Cell Proliferation Assay

Cells were trypsinized, washed, and re-suspended in 1 mL of 1× PBS + 1% EDTA. Cells were incubated with 5 μM of CFSE for 15 min at 37°C in dark. The reaction was stopped by adding 1× PBS + 1% EDTA + 5% FBS; cells were spun down by centrifuging at 500 × *g* for 5 min and re-suspended in 1× PBS. Afterward, cells were quantified, and 150,000 cells were seeded into each well of 6-well dishes, incubated in dark for 3 days, and analyzed by FACS using FACSCalibur (BD Biosciences).

Immunoblotting

Cells were trypsinized, pelleted, washed, and lysed in cold radioimmunoprecipitation assay (RIPA) buffer (with protease inhibitor cocktail) for 5 min, then sonicated. Sonicated lysates were centrifuged at 13,000 rpm at 4°C for 20 min, the clear supernatant was collected and protein concentration was determined by Micro BCA Protein Assay Kit (Thermo Fisher Scientific). Before loading, lysate was mixed with 4× Laemmli buffer and incubated at 95°C for 10 min. For small-scale experiments, cells were washed in 1× PBS and lysed in 2× Laemmli sample buffer and immediately incubated at 95°C for 10 min. Cell lysates were loaded on an SDS-PAGE gel for protein separation by electrophoresis and transferred to nitrocellulose membranes, followed by probing with primary antibodies. Primary antibodies used were as follows: anti-Nogo A and B antibody (N-18) (sc-11027, Santa Cruz Biotechnology), anti-Nogo antibody (I-20) (sc-11034, Santa Cruz Biotechnology), anti-AKT antibody (#9272, Cell Signaling Technology), anti-phospho-AKT antibody (#9271, Cell Signaling Technology), anti-p21 antibody (ab109199, Abcam), anti-phospho-p21 (sc-20220-R, Santa Cruz Biotechnology), anti-phospho-PDK1 antibody (#3438, Cell Signaling Technology), anti-phospho-PI3K antibody (#4228, Cell Signaling Technology), anti-α-tubulin antibody (B-7) (sc-5286, Santa Cruz Biotechnology), anti-acetylated-α-tubulin (6-11B-1) (sc-23950, Santa Cruz Biotechnology), and anti-β-actin antibody (C4) (sc-47778, Santa Cruz Biotechnology). Membranes were incubated with LI-COR IRDye secondary antibodies (dilution 1:10,000) and visualized using Odyssey CLx Imaging System (LI-COR). Internal control was probed from the same membrane in each case.

Immunofluorescence Staining

Cells were trypsinized and grown on coverslips in dishes. Cells were washed with 1× PBS and incubated for 20 min in 4% paraformaldehyde. Coverslips with fixed cells were washed with 1× PBS then permeablized and blocked in 0.1% Triton X-100 (Sigma-Aldrich) and 5% normal goat serum (Jackson ImmunoResearch Laboratories)

for 1 hr. Afterward, cells were incubated at room temperature with primary antibody, washed with 1× PBS, and incubated in secondary antibody for an hour. For visualization of the nucleus, cells were incubated for additional 15 min in 1:1,000 TO-PRO-3 (Life Technologies) in 1× PBS. Coverslips were washed and mounted on glass slides using ProLong Diamond Antifade Mountant (Life Technologies). Primary antibodies were as follows: anti-Nogo A and B antibody (ab47085, Abcam), anti-acetylated-α-tubulin antibody (6-11B-1) (sc-23950, Santa Cruz Biotechnology), anti-α-tubulin antibody (B-7) (sc-5286, Santa Cruz Biotechnology), anti-β-actin antibody (C4) (sc-47778, Santa Cruz Biotechnology). Secondary antibodies were as follows: Alexa Fluor 488 AffiniPure goat anti-rabbit immunoglobulin G (IgG) (Jackson ImmunoResearch Laboratories) and Cy3 AffiniPure goat anti-mouse IgG (Jackson ImmunoResearch Laboratories) were used for immunofluorescence staining.

Imaging

For live cell imaging, cells were trypsinized, then seeded onto 27-mm Nunc glass-bottom dishes (Thermo Fisher Scientific). When required, transient transfection was performed using Lipofectamine 2000 (Life Technologies). To fluorescently label the cellular lipids, cells were incubated in BODIPY FL C_{12} (Molecular Probes) fluorescent fatty acid (a synthetic precursor for various phospholipids that is used to label cellular lipids) at 1:500 dilution in growth media for 4 hr. Live-cell imaging was performed in Fluorbrite DMEM (Gibco) at 37°C and 5% CO_2 using a Zeiss Cell Observer SD Spinning Disk Confocal Microscope equipped with Yokogawa CSU-X1 spinning disk 63× C-Apochromat NA 1.2 and 100× Plan Apochromat NA 1.4 objectives, and 488-nm and 561-nm lasers were used for imaging. Time-course live-cell imaging was performed at a definite focus setting. Images (512 × 512 pixels) were captured by an Evolve 512 EM-CCD camera (Photometrics). ZenBlue image acquisition software (Zeiss) was used for image acquisition. Fixed-cell imaging was performed at Zeiss Meta510 inverted laser scanning confocal microscope equipped with 488 nm, 543 nm, and 633 nm lasers using 63× Apochromat NA 1.2 objective. Images (1,024 × 1,024 pixels) were captured by Zeiss AxioCam MRc camera. ZenBlue image acquisition software (Zeiss) was used for image acquisition. Confocal images were acquired as z stacks, then compiled into a maximal projection and analyzed using ImageJ.[61]

TCGA Patient Tumor Sample Data Analysis

Clinical cancer patient data was obtained from TCGA and cBioPortal (http://www.cbioportal.org) database.[27,28] TCGA lung cancer data, breast cancer data, cervical squamous cell carcinoma, and kidney renal papillary cell carcinoma provincial datasets were used for analysis. Kaplan-Meier survival curves were generated in R. Coxph analysis was performed to calculate hazard ratio. Log rank tests were used for statistics. RTN4 correlation analysis was performed using Pearson correlation. All graphs were generated using R.

In Vivo Experiments

The experimental procedures were governed by the ethics committee at Dalhousie University, Halifax, NS, Canada. Eleven- to twelve-week-old male NOD-SCID mice (NOD.CB17-Prkdcscid/NcrCrl) were obtained from in-house breeding pairs (originally obtained from Charles River Laboratory [Montreal, QC, Canada]). Mice were injected with 2.5 × 10^6 H1299 cells subcutaneously into the left flank. Once tumors reached approximately 40 mm^3, mice were treated with four doses of paclitaxel (7.5 mg/kg mouse), injected subcutaneously, on 4 consecutive days. Tumor volume was calculated by using formula height × width × length × pi/6 as measured with a caliper, and mice were sacrificed at humane tumor endpoints as established by Canadian Council on Animal Care (CCAC) tumor guidelines.

Statistical Analysis

Statistical analyses were performed using a two-tailed Student's t test to compare two samples, and ANOVA analysis was performed to assess more than two samples. A p value less than 0.05 was considered as significant. Kaplan-Meier survival analyses coupled with log rank tests were applied (with 95% confidence interval) for mouse survival analysis.

SUPPLEMENTAL INFORMATION

Supplemental Information includes seven figures and one table and can be found with this article online at https://doi.org/10.1016/j.ymthe.2018.05.026.

AUTHOR CONTRIBUTIONS

G.P.P., S.G., and Z.X. conceived the study. G.P.P. and S.G. designed the study and wrote the manuscript, G.P.P. and R.S. performed the experiment and analyzed the data, B.E.K. and D.C. performed the animal experiment, I.R.S. performed TAG and lipidomic analysis, and J.P.M., P.K., and M.G. performed the proteome and metabolome analysis. S.G. supervised the study.

CONFLICTS OF INTEREST

The authors declare no conflict of interest.

ACKNOWLEDGMENTS

This work was supported by grants from the Canadian Institute of Health Research (CIHR), from the Canadian Breast Cancer Foundation Atlantic (CBCF), and the Breast Cancer Society of Canada (BCSC)/QEII Foundation Awards for breast cancer research through the Beatrice Hunter Cancer Research Institute (BHCRI). The postdoctoral fellowship from the Cancer Research Training Program (CRTP) of BHCRI supported J.P.M. and B.E.K. D.C. is currently funded through a CIHR Doctoral Award and was previously supported by CRTP from BHCRI and the Nova Scotia Health Research Foundation (NSHRF). P.K. is currently supported through NSHRF. I.R.S. was supported by CA168934 from the U.S. NIH (NCI). We thank Dr. Patrick Lee for his support.

REFERENCES

1. Housman, G., Byler, S., Heerboth, S., Lapinska, K., Longacre, M., Snyder, N., and Sarkar, S. (2014). Drug resistance in cancer: an overview. Cancers (Basel) *6*, 1769–1792.

2. Sharma, P., and Allison, J.P. (2015). The future of immune checkpoint therapy. Science *348*, 56–61.

3. Gazdar, A.F., Miyajima, K., Reddy, J., Sathyanarayana, U.G., Shigematsu, H., Suzuki, M., Takahashi, T., and Shivapurkar, N. (2004). Molecular targets for cancer therapy and prevention. Chest *125* (*Suppl 5*), 97S–101S.

4. Polivka, J., Jr., and Janku, F. (2014). Molecular targets for cancer therapy in the PI3K/AKT/mTOR pathway. Pharmacol. Ther. *142*, 164–175.

5. Ahn, D.-G., Sharif, T., Chisholm, K., Pinto, D.M., Gujar, S.A., and Lee, P.W. (2015). Ras transformation results in cleavage of reticulon protein Nogo-B that is associated with impairment of IFN response. Cell Cycle *14*, 2301–2310.

6. Chen, M.S., Huber, A.B., van der Haar, M.E., Frank, M., Schnell, L., Spillmann, A.A., Christ, F., and Schwab, M.E. (2000). Nogo-A is a myelin-associated neurite outgrowth inhibitor and an antigen for monoclonal antibody IN-1. Nature *403*, 434–439.

7. Schwab, M.E. (2010). Functions of Nogo proteins and their receptors in the nervous system. Nat. Rev. Neurosci. *11*, 799–811.

8. Sutendra, G., Dromparis, P., Wright, P., Bonnet, S., Haromy, A., Hao, Z., McMurtry, M.S., Michalak, M., Vance, J.E., Sessa, W.C., and Michelakis, E.D. (2011). The role of Nogo and the mitochondria-endoplasmic reticulum unit in pulmonary hypertension. Sci. Transl. Med. *3*, 88ra55.

9. Acevedo, L., Yu, J., Erdjument-Bromage, H., Miao, R.Q., Kim, J.-E., Fulton, D., Tempst, P., Strittmatter, S.M., and Sessa, W.C. (2004). A new role for Nogo as a regulator of vascular remodeling. Nat. Med. *10*, 382–388.

10. Cantalupo, A., Zhang, Y., Kothiya, M., Galvani, S., Obinata, H., Bucci, M., Giordano, F.J., Jiang, X.C., Hla, T., and Di Lorenzo, A. (2015). Nogo-B regulates endothelial sphingolipid homeostasis to control vascular function and blood pressure. Nat. Med. *21*, 1028–1037.

11. Wright, P.L., Yu, J., Di, Y.P.P., Homer, R.J., Chupp, G., Elias, J.A., Cohn, L., and Sessa, W.C. (2010). Epithelial reticulon 4B (Nogo-B) is an endogenous regulator of Th2-driven lung inflammation. J. Exp. Med. *207*, 2595–2607.

12. Rodríguez-Feo, J.A., Puerto, M., Fernández-Mena, C., Verdejo, C., Lara, J.M., Díaz-Sánchez, M., Álvarez, E., Vaquero, J., Marín-Jiménez, I., Bañares, R., and Menchén, L. (2015). A new role for reticulon-4B/NOGO-B in the intestinal epithelial barrier function and inflammatory bowel disease. Am. J. Physiol. Gastrointest. Liver Physiol. *308*, G981–G993.

13. Yu, J., Fernández-Hernando, C., Suarez, Y., Schleicher, M., Hao, Z., Wright, P.L., DiLorenzo, A., Kyriakides, T.R., and Sessa, W.C. (2009). Reticulon 4B (Nogo-B) is necessary for macrophage infiltration and tissue repair. Proc. Natl. Acad. Sci. USA *106*, 17511–17516.

14. Di Lorenzo, A., Manes, T.D., Davalos, A., Wright, P.L., and Sessa, W.C. (2011). Endothelial reticulon-4B (Nogo-B) regulates ICAM-1-mediated leukocyte transmigration and acute inflammation. Blood *117*, 2284–2295.

15. Zhang, Y., Huang, Y., Cantalupo, A., Azevedo, P.S., Siragusa, M., Bielawski, J., Giordano, F.J., and Di Lorenzo, A. (2016). Endothelial Nogo-B regulates sphingolipid biosynthesis to promote pathological cardiac hypertrophy during chronic pressure overload. JCI Insight *1*, e85484.

16. Tashiro, K., Satoh, A., Utsumi, T., Chung, C., and Iwakiri, Y. (2013). Absence of Nogo-B (reticulon 4B) facilitates hepatic stellate cell apoptosis and diminishes hepatic fibrosis in mice. Am. J. Pathol. *182*, 786–795.

17. Rodríguez-Feo, J.A., Gallego-Delgado, J., Puerto, M., Wandosell, F., and Osende, J. (2016). Reticulon-4B/Nogo-B acts as a molecular linker between microtubules and actin cytoskeleton in vascular smooth muscle cells. Biochim. Biophys. Acta *1863*, 1985–1995.

18. Schanda, K., Hermann, M., Stefanova, N., Gredler, V., Bandtlow, C., and Reindl, M. (2011). Nogo-B is associated with cytoskeletal structures in human monocyte-derived macrophages. BMC Res. Notes *4*, 6.

19. Miao, R.Q., Gao, Y., Harrison, K.D., Prendergast, J., Acevedo, L.M., Yu, J., Hu, F., Strittmatter, S.M., and Sessa, W.C. (2006). Identification of a receptor necessary for Nogo-B stimulated chemotaxis and morphogenesis of endothelial cells. Proc. Natl. Acad. Sci. USA *103*, 10997–11002.

20. Zhu, B., Chen, S., Hu, X., Jin, X., Le, Y., Cao, L., Yuan, Z., Lin, Z., Jiang, S., Sun, L., and Yu, L. (2017). Knockout of the Nogo-B Gene Attenuates Tumor Growth and Metastasis in Hepatocellular Carcinoma. Neoplasia *19*, 583–593.

21. Bateman, L.A., Nguyen, T.B., Roberts, A.M., Miyamoto, D.K., Ku, W.-M., Huffman, T.R., Petri, Y., Heslin, M.J., Contreras, C.M., Skibola, C.F., et al. (2017). Chemoproteomics-enabled covalent ligand screen reveals a cysteine hotspot in reticulon 4 that impairs ER morphology and cancer pathogenicity. Chem. Commun. (Camb.) *53*, 7234–7237.

22. Lasserre, R., Guo, X.-J., Conchonaud, F., Hamon, Y., Hawchar, O., Bernard, A.-M., Soudja, S.M., Lenne, P.F., Rigneault, H., Olive, D., et al. (2008). Raft nanodomains contribute to Akt/PKB plasma membrane recruitment and activation. Nat. Chem. Biol. *4*, 538–547.

23. Scheid, M.P., and Woodgett, J.R. (2003). Unravelling the activation mechanisms of protein kinase B/Akt. FEBS Lett. *546*, 108–112.

24. Vivanco, I., and Sawyers, C.L. (2002). The phosphatidylinositol 3-Kinase AKT pathway in human cancer. Nat. Rev. Cancer *2*, 489–501.

25. Vanhaesebroeck, B., Stephens, L., and Hawkins, P. (2012). PI3K signalling: the path to discovery and understanding. Nat. Rev. Mol. Cell Biol. *13*, 195–203.

26. Fruman, D.A., and Rommel, C. (2014). PI3K and cancer: lessons, challenges and opportunities. Nat. Rev. Drug Discov. *13*, 140–156.

27. Cerami, E., Gao, J., Dogrusoz, U., Gross, B.E., Sumer, S.O., Aksoy, B.A., Jacobsen, A., Byrne, C.J., Heuer, M.L., Larsson, E., et al. (2012). The cBio cancer genomics portal: an open platform for exploring multidimensional cancer genomics data. Cancer Discov. *2*, 401–404.

28. Gao, J., Aksoy, B.A., Dogrusoz, U., Dresdner, G., Gross, B., Sumer, S.O., Sun, Y., Jacobsen, A., Sinha, R., Larsson, E., et al. (2013). Integrative analysis of complex cancer genomics and clinical profiles using the cBioPortal. Sci. Signal. *6*, pl1.

29. Clements, D.R., Murphy, J.P., Sterea, A., Kennedy, B.E., Kim, Y., Helson, E., Almasi, S., Holay, N., Konda, P., Paulo, J.A., et al. (2017). Quantitative Temporal in Vivo Proteomics Deciphers the Transition of Virus-Driven Myeloid Cells into M2 Macrophages. J. Proteome Res. *16*, 3391–3406.

30. Weekes, M.P., Tomasec, P., Huttlin, E.L., Fielding, C.A., Nusinow, D., Stanton, R.J., Wang, E.C., Aicheler, R., Murrell, I., Wilkinson, G.W., et al. (2014). Quantitative temporal viromics: an approach to investigate host-pathogen interaction. Cell *157*, 1460–1472.

31. Supek, F., Bošnjak, M., Škunca, N., and Šmuc, T. (2011). REVIGO Summarizes and Visualizes Long Lists of Gene Ontology Terms. PLoS ONE *6*, e21800.

32. Abbas, T., and Dutta, A. (2009). p21 in cancer: intricate networks and multiple activities. Nat. Rev. Cancer *9*, 400–414.

33. Manning, B.D., and Cantley, L.C. (2007). AKT/PKB signaling: navigating downstream. Cell *129*, 1261–1274.

34. Pernet, V., Joly, S., Christ, F., Dimou, L., and Schwab, M.E. (2008). Nogo-A and myelin-associated glycoprotein differently regulate oligodendrocyte maturation and myelin formation. J. Neurosci. *28*, 7435–7444.

35. Saher, G., Brügger, B., Lappe-Siefke, C., Möbius, W., Tozawa, R., Wehr, M.C., Wieland, F., Ishibashi, S., and Nave, K.A. (2005). High cholesterol level is essential for myelin membrane growth. Nat. Neurosci. *8*, 468–475.

36. Yuan, M., Breitkopf, S.B., Yang, X., and Asara, J.M. (2012). A positive/negative ion-switching, targeted mass spectrometry-based metabolomics platform for bodily fluids, cells, and fresh and fixed tissue. Nat. Protoc. *7*, 872–881.

37. Gault, C.R., Obeid, L.M., and Hannun, Y.A. (2010). An overview of sphingolipid metabolism: from synthesis to breakdown. Adv. Exp. Med. Biol. *688*, 1–23.

38. Al-Bassam, J., and Corbett, K.D. (2012). α-Tubulin acetylation from the inside out. Proc. Natl. Acad. Sci. USA *109*, 19515–19516.

39. Boggs, A.E., Vitolo, M.I., Whipple, R.A., Charpentier, M.S., Goloubeva, O.G., Ioffe, O.B., Tuttle, K.C., Slovic, J., Lu, Y., Mills, G.B., and Martin, S.S. (2015). α-Tubulin acetylation elevated in metastatic and basal-like breast cancer cells promotes microtentacle formation, adhesion, and invasive migration. Cancer Res. *75*, 203–215.

40. Rowinsky, E.K., Cazenave, L.A., and Donehower, R.C. (1990). Taxol: a novel investigational antimicrotubule agent. J. Natl. Cancer Inst. *82*, 1247–1259.

41. Hu, L., Hofmann, J., Lu, Y., Mills, G.B., and Jaffe, R.B. (2002). Inhibition of phosphatidylinositol 3′-kinase increases efficacy of paclitaxel in in vitro and in vivo ovarian cancer models. Cancer Res. *62*, 1087–1092.

42. Liu, Z., Zhu, G., Getzenberg, R.H., and Veltri, R.W. (2015). The Upregulation of PI3K/Akt and MAP Kinase Pathways is Associated with Resistance of Microtubule-Targeting Drugs in Prostate Cancer. J. Cell. Biochem. *116*, 1341–1349.

43. Avan, A., Narayan, R., Giovannetti, E., and Peters, G.J. (2016). Role of Akt signaling in resistance to DNA-targeted therapy. World J. Clin. Oncol. *7*, 352–369.

44. Kreisberg, J.I., Malik, S.N., Prihoda, T.J., Bedolla, R.G., Troyer, D.A., Kreisberg, S., and Ghosh, P.M. (2004). Phosphorylation of Akt (Ser473) is an excellent predictor of poor clinical outcome in prostate cancer. Cancer Res. *64*, 5232–5236.

45. Wesley, U.V., Hatcher, J.F., and Dempsey, R.J. (2015). Sphingomyelin synthase 1 regulates Neuro-2a cell proliferation and cell cycle progression through modulation of p27 expression and Akt signaling. Mol. Neurobiol. *51*, 1530–1541.

46. Tafesse, F.G., Huitema, K., Hermansson, M., van der Poel, S., van den Dikkenberg, J., Uphoff, A., Somerharju, P., and Holthuis, J.C. (2007). Both sphingomyelin synthases SMS1 and SMS2 are required for sphingomyelin homeostasis and growth in human HeLa cells. J. Biol. Chem. *282*, 17537–17547.

47. Arbiser, J.L., Kau, T., Konar, M., Narra, K., Ramchandran, R., Summers, S.A., Vlahos, C.J., Ye, K., Perry, B.N., Matter, W., et al. (2007). Solenopsin, the alkaloidal component of the fire ant (Solenopsis invicta), is a naturally occurring inhibitor of phosphatidylinositol-3-kinase signaling and angiogenesis. Blood *109*, 560–565.

48. Karlsson, I., Zhou, X., Thomas, R., Smith, A.T., Bonner, M.Y., Bakshi, P., Banga, A.K., Bowen, J.P., Qabaja, G., Ford, S.L., et al. (2015). Solenopsin A and analogs exhibit ceramide-like biological activity. Vasc. Cell *7*, 5.

49. Akamata, K., Wei, J., Bhattacharyya, M., Cheresh, P., Bonner, M.Y., Arbiser, J.L., Raparia, K., Gupta, M.P., Kamp, D.W., and Varga, J. (2016). SIRT3 is attenuated in systemic sclerosis skin and lungs, and its pharmacologic activation mitigates organ fibrosis. Oncotarget *7*, 69321–69336.

50. Matrone, M.A., Whipple, R.A., Balzer, E.M., and Martin, S.S. (2010). Microtentacles tip the balance of cytoskeletal forces in circulating tumor cells. Cancer Res. *70*, 7737–7741.

51. Siudeja, K., Srinivasan, B., Xu, L., Rana, A., de Jong, J., Nollen, E.A.A., Jackowski, S., Sanford, L., Hayflick, S., and Sibon, O.C. (2011). Impaired Coenzyme A metabolism affects histone and tubulin acetylation in Drosophila and human cell models of pantothenate kinase associated neurodegeneration. EMBO Mol. Med. *3*, 755–766.

52. Fujiwara, Y., Hosokawa, Y., Watanabe, K., Tanimura, S., Ozaki, K., and Kohno, M. (2007). Blockade of the phosphatidylinositol-3-kinase-Akt signaling pathway enhances the induction of apoptosis by microtubule-destabilizing agents in tumor cells in which the pathway is constitutively activated. Mol. Cancer Ther. *6*, 1133–1142.

53. Wang, W., Goswami, S., Lapidus, K., Wells, A.L., Wyckoff, J.B., Sahai, E., Singer, R.H., Segall, J.E., and Condeelis, J.S. (2004). Identification and testing of a gene expression signature of invasive carcinoma cells within primary mammary tumors. Cancer Res. *64*, 8585–8594.

54. Goley, E.D., and Welch, M.D. (2006). The ARP2/3 complex: an actin nucleator comes of age. Nat. Rev. Mol. Cell Biol. *7*, 713–726.

55. Rotty, J.D., Wu, C., and Bear, J.E. (2013). New insights into the regulation and cellular functions of the ARP2/3 complex. Nat. Rev. Mol. Cell Biol. *14*, 7–12.

56. Orr, G.A., Verdier-Pinard, P., McDaid, H., and Horwitz, S.B. (2003). Mechanisms of Taxol resistance related to microtubules. Oncogene *22*, 7280–7295.

57. Merrill, A.H.J., Jr., Sullards, M.C., Allegood, J.C., Kelly, S., and Wang, E. (2005). Sphingolipidomics: high-throughput, structure-specific, and quantitative analysis of sphingolipids by liquid chromatography tandem mass spectrometry. Methods *36*, 207–224.

58. Hutchins, P.M., Barkley, R.M., and Murphy, R.C. (2008). Separation of cellular nonpolar neutral lipids by normal-phase chromatography and analysis by electrospray ionization mass spectrometry. J. Lipid Res. *49*, 804–813.

59. Ting, L., Rad, R., Gygi, S.P., and Haas, W. (2011). MS3 eliminates ratio distortion in isobaric multiplexed quantitative proteomics. Nat. Methods *8*, 937–940.

60. Murphy, J.P., Stepanova, E., Everley, R.A., Paulo, J.A., and Gygi, S.P. (2015). Comprehensive Temporal Protein Dynamics during the Diauxic Shift in Saccharomyces cerevisiae. Mol. Cell. Proteomics *14*, 2454–2465.

61. Schneider, C.A., Rasband, W.S., and Eliceiri, K.W. (2012). NIH Image to ImageJ: 25 years of image analysis. Nat. Methods *9*, 671–675.